JMEPEG (2014) 23:125–132
DOI: 10.1007/s11665-013-0756-z

1059-9495/$19.00

Effects of Flux Precoating and Process Parameter on Welding Performance of Inconel 718 Alloy TIG Welds

Hsuan-Liang Lin, Tong-Min Wu, and Ching-Min Cheng

(Submitted January 20, 2012; in revised form August 30, 2013; published online October 22, 2013)

The purpose of this study is to investigate the effect of activating flux on the depth-to-width ratio (DWR) and hot cracking susceptibility of Inconel 718 alloy tungsten inert gas (TIG) welds. The Taguchi method is employed to investigate the welding parameters that affect the DWR of weld bead and to achieve optimal conditions in the TIG welds that are coated with activating flux in TIG (A-TIG) process. There are eight single-component fluxes used in the initial experiment to evaluate the penetration capability of A-TIG welds. The experimental results show that the Inconel 718 alloy welds precoated with 50% SiO_2 and 50% MoO_3 flux were provided with better welding performance such as DWR and hot cracking susceptibility. The experimental procedure of TIG welding process using mixed-component flux and optimal conditions not only produces a significant increase in DWR of weld bead, but also decreases the hot cracking susceptibility of Inconel 718 alloy welds.

Keywords activating flux, hot cracking, Inconel 718 alloy, TIG welding, welds morphology

1. Introduction

Inconel 718 alloy is one of the most widely used Ni-based alloys due to its superior mechanical property and oxidation resistance at high temperature. It has been used in gas turbines, aircraft engines, and nuclear plants. Electron beam (EB), laser beam (LB), and tungsten inert gas (TIG) welding processes were known to play important roles in aerospace, military, power plant, and automotive industries. Many researches studying EB and LB of Inconel 718 alloy have been performed because of the high depth-to-width (DWR) ratio of weld bead geometry, rapid welding speeds, narrow heat-affected zone (HAZ), low distortion, and so on (Ref 1-4). In contrast, a few published reports that are available on TIG welding of Inconel 718 alloy focus on investigation and selection of welding parameters for obtaining optimal welding performance. The TIG welding is one of the mainly applied welding processes in industry to stainless steels and nonferrous metals and its alloys such as aluminum, magnesium, and Ni-based alloys for high-quality weld and low investment (Ref 5). The TIG welding quality is strongly characterized by the weld bead geometry. The weld bead geometry plays an important role in determining the mechanical properties of the weld (Ref 6, 7). However, the relatively shallow penetration capability and low productivity are the main disadvantage in the TIG welding process. Achieving full penetration of welds and increasing productivity are the main objectives in the welding industry. In order to achieve single-pass welds with no edge preparation, instead of multipass procedures, one of the most notable techniques is to use activating flux in the TIG (A-TIG) welding process (Ref 8). Huang et al. (Ref 9) and Yang et al. (Ref 10) proved that oxide flux SiO_2 cause an important increase in penetration on JIS SUS 304 stainless steel in the bead-on-plate A-TIG welding process. In addition, Chern et al. (Ref 11) proved that using oxide fluxes of SiO_2, MoO_3, and Cr_2O_3 not only increased the penetration capability, but also improved the mechanical properties of grade 2205 duplex stainless steel in the A-TIG welding process.

The majority of weldability tests have been developed to evaluate the susceptibility of the base materials to crack. The purpose of these tests is to reduce or eliminate the formation of these defects during fabrication or service. Hot cracking occurs during weld solidification and can occur in the weld metal or in the HAZ. Hot cracking is caused by low melting temperature constituents, in addition to tensile stress on the weld (Ref 12). In general, lower heat input reduces the volume of weld metal that undergoes shrinkage during cooling and results in less overall contraction in the HAZ during cooling. It is well known that minimizing weld heat input can be an effective method for eliminating or minimizing HAZ liquation cracking. An experiment using plasma arc welding (Ref 13) was designed to study the effect of welding energy input and its variables such as welding current and speed on the tendency to crack of Inconel 713C alloy welds. The experimental results demonstrated that the tendency to crack decreased with increasing energy input and decreasing welding speed. HAZ weld cracking is minimized by optimizing welding current and speed as well as energy input. In addition, Gordine (Ref 14) demonstrated that the susceptibility to microfissuring of Inconel 718 welds was greater under TIG welding conditions of low heat input. Microfissuring in the HAZ of Inconel 718 welds can be prevented by using material solution treated below 1950 F and by avoiding low weld heat

Hsuan-Liang Lin, Department of Vehicle Engineering, Army Academy R.O.C., Taoyuan, Taiwan; **Tong-Min Wu**, Department of Mechanical Engineering, National Chiao Tung University, Hsinchu, Taiwan; and **Ching-Min Cheng**, Department of Mechatronic Technology, National Taiwan Normal University, Taipei, Taiwan. Contact e-mail: alaniin@ms47.hinet.net.

Table 1 Chemical concentration of each element in Inconel 718 alloy

Element	Ni	Cr	Nb + Ta	Mo	Ti	Al	Co	C	Mn	Si	Fe
Wt.%	55.0	21.0	5.5	3.3	1.15	0.8	1.0	0.05	0.35	0.35	Balance

inputs. Many researchers (Ref 9, 10) proved that the voltage of welding arc for specimens with precoated flux increase by about 15-53% compared with specimens without precoating flux. Since the heat input is proportional to the arc voltage, precoated activating flux on Inconel 718 alloy specimens has the positive effect of increasing the heat input and reducing the hot cracking susceptibility during the TIG welding process. The purpose of this study is to investigate the effects of both the flux precoating and the TIG welding parameters on the hot cracking susceptibility and weld bead geometry of the Inconel 718 welds. First, the single- and mixed-component fluxes were precoated on Inconel 718 alloy specimens to evaluate the effects of weld bead geometry, voltage of welding arc, and hot cracking susceptibility. Then, the Taguchi method was used to optimize the weld bead geometry and analyze the effect of welding parameters of Inconel 718 welds in the A-TIG welding process.

2. Experimental Procedure

Inconel 718 alloy sheets with dimension $50 \times 100 \times 6.35$ mm^3 were prepared for this study; its chemical composition is listed in Table 1. Before TIG welding using a EWTh-2 electrode to produce a bead-on-plate weld, an activating flux that contains oxide powder was mixed with methanol to produce paint-like consistency, and a layer thickness of approximately 0.2 mm is applied to the surface of base metal to be welded by means of a brush, as shown in Fig. 1(a). The single-component fluxes used in the initial experiment were SiO_2, NiO, MoO_3, Cr_2O_3, TiO_2, MnO_2, ZnO, and MoS_2. The welding parameters used in the initial experiment are given in Table 2. In this study, measurements of the weld bead geometry were performed for evaluation of the quality of Inconel 718 alloy welds. In this study, the width of weld bead and the depth of penetration were considered to describe the weld bead geometry. The DWR ratio of the weld bead geometry of each specimen was selected as the quality characteristic of TIG welding process. An optical microscope was used to measure the depth and width of weld bead geometry of each specimen. All metallographic specimens were prepared by mechanical lapping, grinding, and polishing to a 0.3-μm finish, followed by etching in a solution containing 2 g of $CuCl_2$, 40 mL of CH_3OH, and 35 mL of HCl. The varestraint test is the most common test used to evaluate hot cracking sensitivity. The spot varestraint test is a modification of the earlier varestraint test (Ref 12). In this study, the hot cracking susceptibility was evaluated using a spot varestraint test machine developed by the authors as shown in Fig. 2. Welding conditions of spot varestraint test were 80 A welding current with 7 s arc time on 3-mm-thick Inconel 718 alloy plate, and the arc length was maintained at

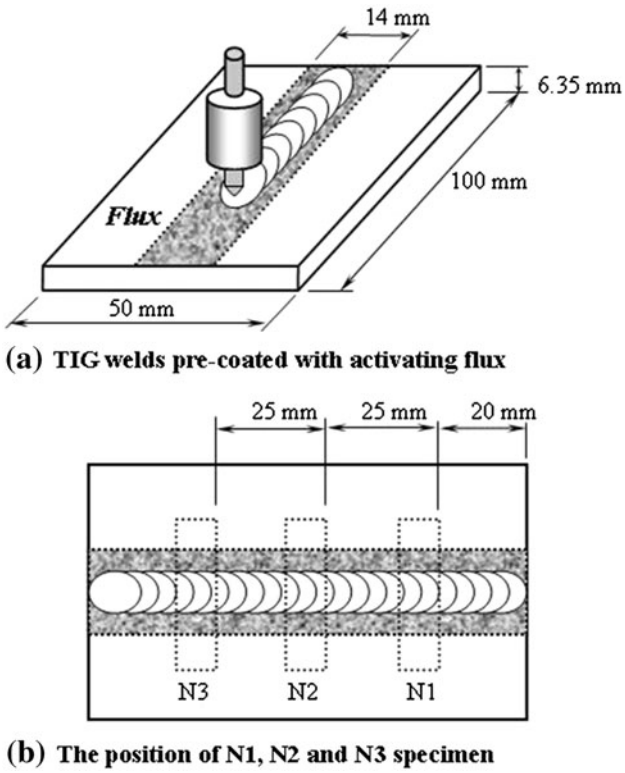

Fig. 1 Schematic diagram of the TIG welds precoated with activating flux

Table 2 Welding parameters for initial experiments

Welding current	170 A
Travel speed	150 mm/min
Arc length	2.0 mm
Diameter of electrode (EWTh-2 type)	3.2 mm
Angle of electrode tip	60°
Flow rate of shield gas (99.9% Argon gas)	14 L/min

1.6 mm. The augmented tangential strain imparted to the surface of the specimens is 5%. The flux powder was uniformly dispersed with methanol to produce paint-like consistency and brush coating was applied on the Inconel 718 alloy plate surfaces as shown in Fig. 2(a). A TIG spot weld is performed in the center of the topside of the specimen. The arc is then extinguished and the load immediately applied to force the sample to conform to the die block. Hot cracking occurred in both the welded metal and the HAZ. The total cracking length (TCL) was recorded to evaluate the hot cracking susceptibility of Inconel 718 alloy welding specimens coated with activating flux.

3. Results and Discussion

3.1 Effect of Flux Precoating on Weld Bead Geometry

The previous studies (Ref 15-18) have revealed that the base metal precoated with activating fluxes led to an increased penetration of weld bead due to two types of actions: namely, the Marangoni flow effect, and the electric arc behavior. The first action is that the activating fluxes produce a positive surface tension temperature coefficient which changes the direction of the flow in the weld pool from outward to inward, thereby producing a relatively deep and narrow weld. On the other hand, the fluxes may influence the arc plasma. The dissociation and ionization of flux elements may induce a constriction of the electric arc. Figure 3 shows the DWRs of weld bead geometry made by conventional TIG welding and the A-TIG welding processes with different single-component fluxes of the Inconel 718 alloy. The penetration capability of A-TIG welds was obviously higher than that of the welds without flux. Based on the higher DWR of specimens as shown in Fig. 3, four single-component fluxes were selected to mix with each other using 50 wt.%. The mixed-component fluxes were SiO_2-MoO_3, SiO_2-NiO, MoO_3-NiO, SiO_2-MoS_2, MoS_2-NiO, and MoS_2-MoO_3, and the mixed-component fluxes were used for investigating their effect on the DWRs of specimens. Figure 4 shows the DWR of weld bead geometry using the mixed-component fluxes. The DWRs of welds precoated with mixed-component flux were higher than those of the welds precoated with single-component fluxes in A-TIG welding, with the oxide 50% SiO_2 + 50% MoO_3 being the most significant.

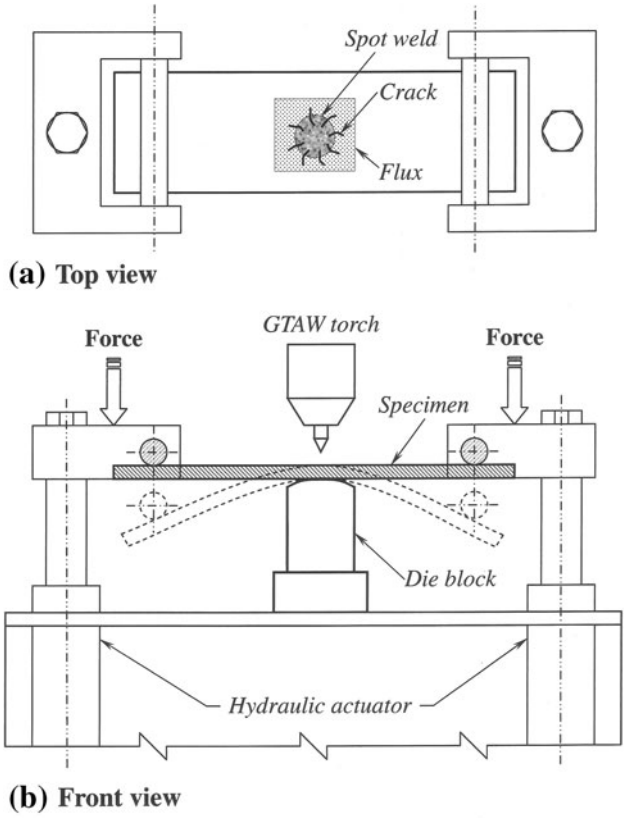

Fig. 2 Schematic diagram of the spot varestraint test machine

3.2 Effect of Flux Precoating on Voltage of Welding Arc

To compare the effect of activating fluxes, voltage of welding arc measurement was conducted on Inconel 718 alloy welds that were precoated with single- and mixed-component fluxes, respectively. Figures 3 and 4 show the effect of A-TIG on average voltage of welding arc. It is found that the voltage of welding arc increases when the TIG welding produced with activating flux was performed, exception being the process involving coating with single-component fluxes TiO_2 and

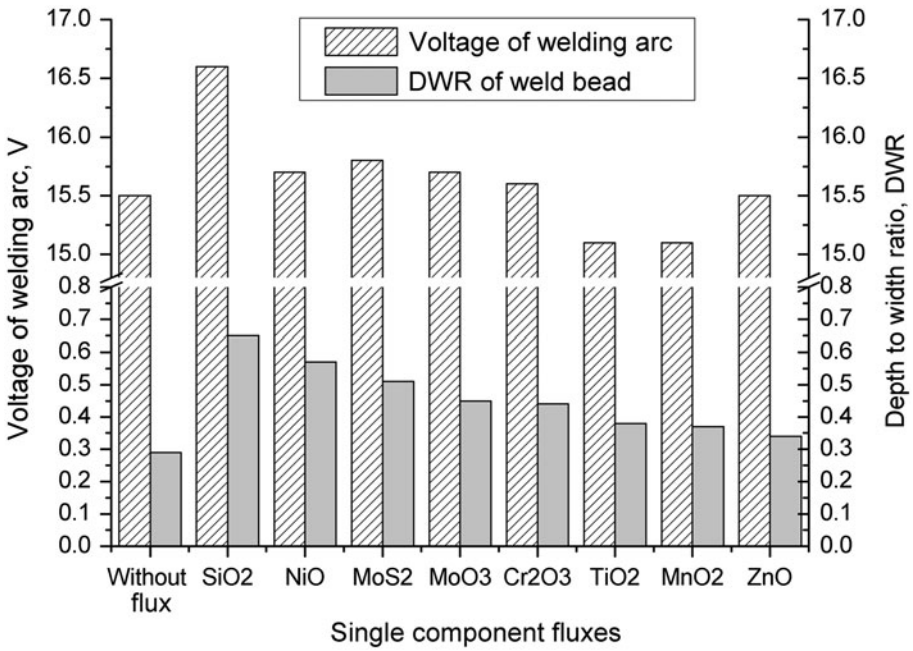

Fig. 3 Effects of single-component fluxes on welding arc voltage and penetration

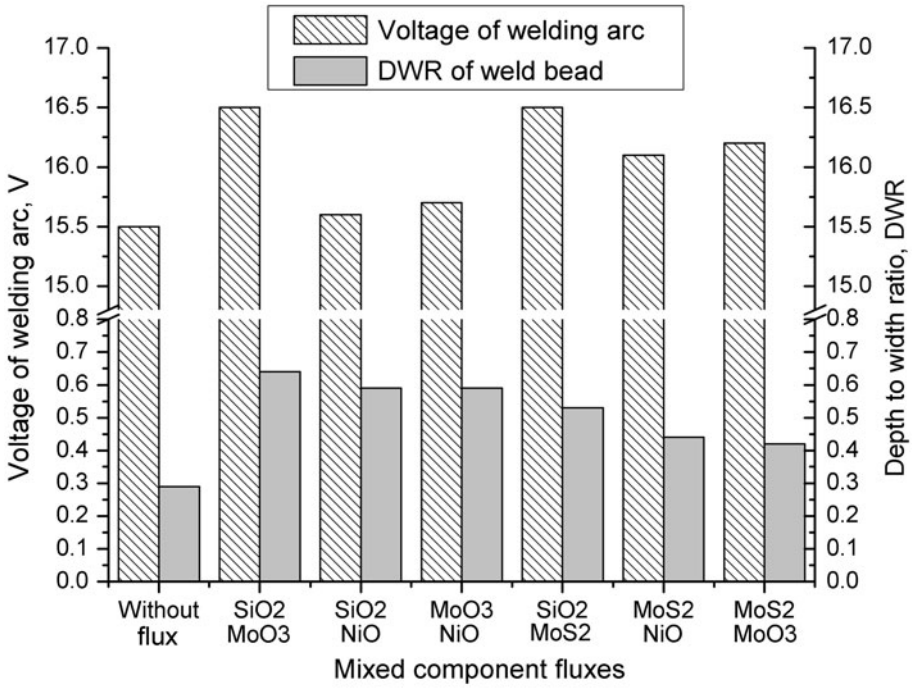

Fig. 4 Effects of mixed-component fluxes on welding arc voltage and penetration

MnO_2. The fluxes SiO_2, 50% SiO_2 + 50% MoO_3, and 50% SiO_2 + 50% MnS_2 have significant effects on the voltage of TIG welding arc. Since the heat input is proportional to the voltage of welding arc, the applying activating flux has the positive effect of increasing the heat input during the TIG welding process.

3.3 Effect of Flux Precoating on Hot Cracking

The crack morphology of the Inconel 718 alloy welds precoated with activating fluxes tested via the spot varestraint test is shown in Fig. 5. The hot cracking resistance of the A-TIG welding is higher than that of the conventional TIG welding. Recent research (Ref 13, 14) has shown that the heat input also significantly affects hot cracking, indicating that the higher energy density decreases the cracking susceptibility. According to these results, the A-TIG welding can produce deeper penetration welds due to higher current density. Therefore, the hot cracking susceptibility of Inconel 718 alloy welds was reduced when activating flux was precoated on the TIG welds. In the present study, reduction in hot cracking susceptibility is the most significant effect realized with the use of 50% SiO_2 + 50% MoO_3 mixed-component flux.

3.4 Determination of Optimal Welding Process Parameters

In order to optimize the weld bead geometry of Inconel 718 welds, as well as analyze the effect of welding parameters in the A-TIG process, the Taguchi was adopted in this study. The previous experiment (Ref 19) showed that the most significant parameters for DWR of weld bead geometry are welding current, travel speed of the welding torch, and electrode angle in TIG welding process. In addition, a mixed-component flux that contains 50% SiO_2 and 50% MoO_3 has the most significant effect on penetration capability and hot cracking susceptibility of Inconel 718 alloy welds as shown in Fig. 4 and 5, respectively, and the weight ratio of oxide powder SiO_2 and MoO_3 was selected as a control factor. The parameters at the different levels are listed in Table 3. The each position of N1, N2, and N3 specimenS on each specimen was selected as the noise factor, as shown in Fig. 1(b). One two-level and five three-level control factors were considered. The L18 ($2^1 \times 3^7$) orthogonal array (OA) that has 17 degrees of freedom was employed in this study, as shown in Table 4. There are $18 \times 2 = 36$ separate test conditions; two repetitions for each trial were planned in this experimental arrangement. The DWR of weld bead, as discussed earlier, is a higher-is-better (HB) quality characteristic. The signal-to-noise ratios (SNR), which condense multiple data points in a trial, depend on the characteristic that is being evaluated (Ref 20). The equation for the SNR of HB characteristic is

$$\mathrm{SNR} = -10 \log \left(\frac{1}{n} \sum_{i=1}^{n} \frac{1}{y_i^2} \right), \qquad \text{(Eq 1)}$$

where n is the number of tests in a trial (which equals number of repetitions regardless of noise levels) and y_i is the DWR of weld bead geometry of the specimens. The value of n is six in this study. The SNRs corresponding to the DWR of weld bead of each trial are shown in Table 4. Figure 6 plots the SNR graph obtained from Table 4. The

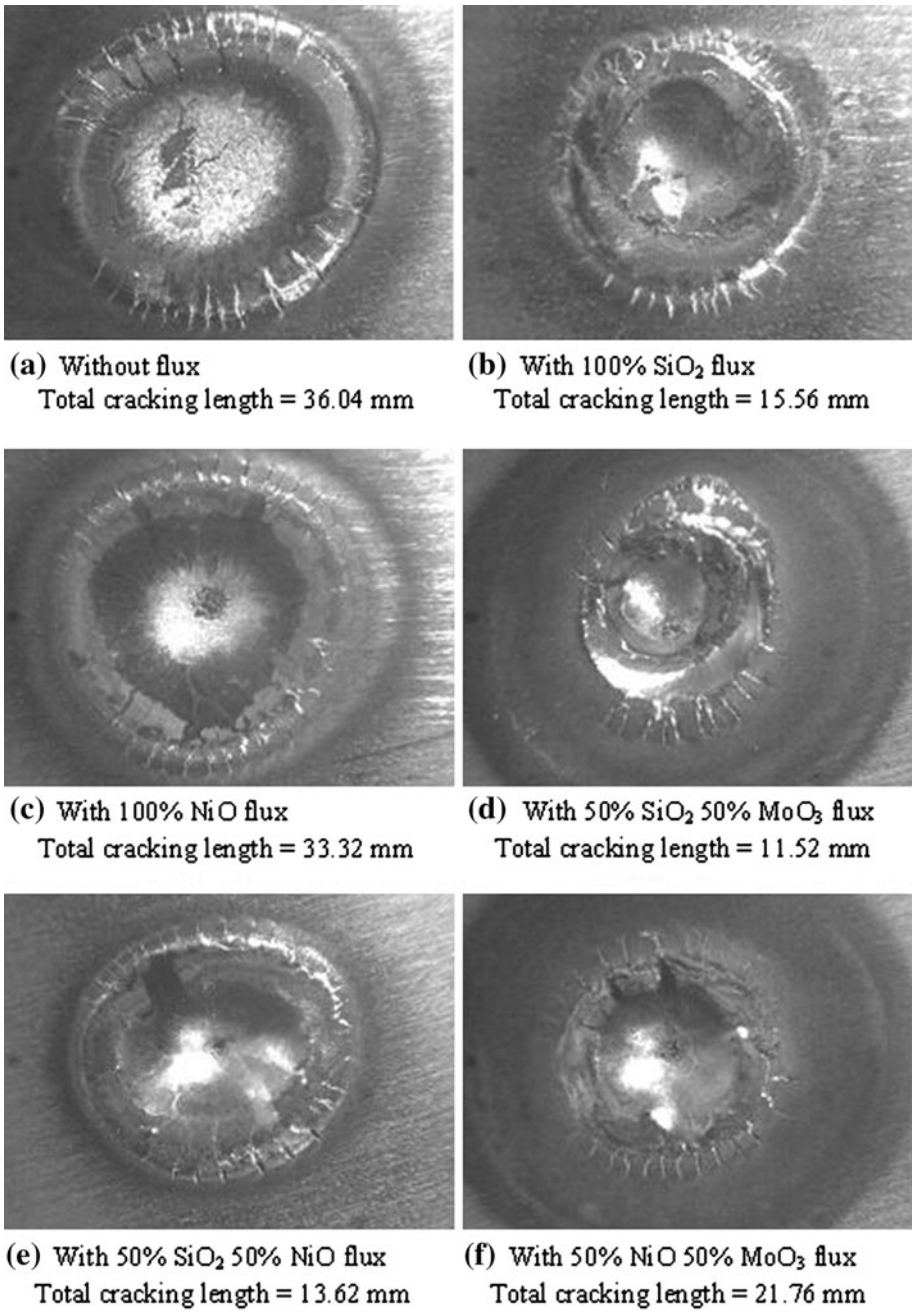

Fig. 5 Effect of activating fluxes on hot cracking susceptibility

Table 3 Control factors and their levels

Factor	Process parameter	Level 1	Level 2	Level 3
A	Arc length, mm	2.0	2.5	…
B	Travel speed, mm/min	150	160	170
C	Flow rate of shield gas, L/min	8	11	14
D	Welding current, A	170	180	190
E	Angle of electrode tip, °	45	60	75
F	Weight ratio of mixed flux	75% SiO_2 25% MoO_3	50% SiO_2 50% MoO_3	25% SiO_2 75% MoO_3

Table 4 Summary of experimental layout and experimental data

Trial no.	Control factors						DWR ratio	
	A	B	C	D	E	F	Average, DWR	SNR, dB
1	1	1	1	1	1	1	0.688	−3.387
2	1	1	2	2	2	2	0.690	−3.248
3	1	1	3	3	3	3	0.829	−1.649
4	1	2	1	1	2	2	0.723	−2.902
5	1	2	2	2	3	3	0.817	−1.786
6	1	2	3	3	1	1	0.628	−4.082
7	1	3	1	2	1	3	0.572	−4.907
8	1	3	2	3	2	1	0.645	−3.834
9	1	3	3	1	3	2	0.941	−0.541
10	2	1	1	3	3	2	0.758	−2.456
11	2	1	2	1	1	3	0.537	−5.407
12	2	1	3	2	2	1	0.592	−4.579
13	2	2	1	2	3	1	0.866	−1.383
14	2	2	2	3	1	2	0.639	−3.940
15	2	2	3	1	2	3	0.531	−5.523
16	2	3	1	3	2	3	0.525	−5.666
17	2	3	2	1	3	1	0.655	−3.731
18	2	3	3	2	1	2	0.651	−3.790

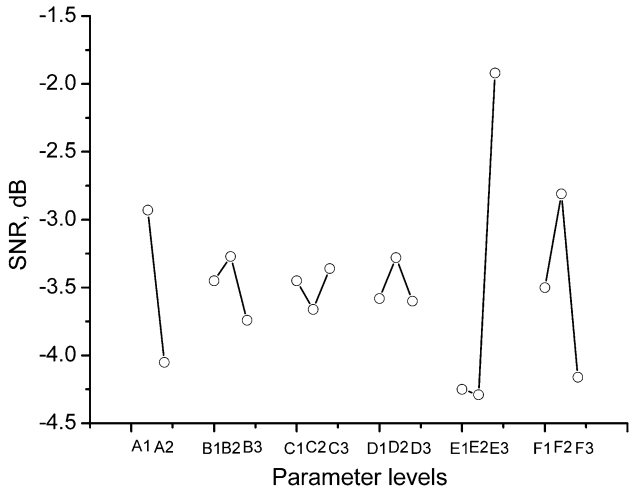

Fig. 6 SNR graph for the DWR ratio of weld bead

Table 5 Results of ANOVA for DWR ratio

Factor	DOF (a)	Sum of square	Mean square	*F*-test	Pure sum of square	Contribution (%)
A	1	5.71	5.712	15.980	5.354	14.29
B	2	0.69 (b)	…	…	…	…
C	2	0.28 (b)	…	…	…	…
D	2	0.39 (b)	…	…	…	…
E	2	22.05	11.026	30.846	21.336	56.95
F	2	5.41	2.707	7.575	4.700	12.54
Error	6	2.93 (b)	…	…	…	…
$Error_{(pooled)}$	(12)	(4.289)	(0.357)		6.08	16.22
Total	17	37.47			37.47	100

(a) DOF indicates the degree of freedom
(b) The factors are treated as pooled error

optimal conditions of parameter levels in the A-TIG welding process, $A_1B_2C_3D_2E_3F_2$, are obtained from Fig. 6. The purpose of the analysis of variance (ANOVA) was to identify which welding parameters significantly affected the weld bead geometry. Table 5 shows the results of the ANOVA for the DWR of the specimens in this study. The arc length, the angle of electrode tip, and the weight ratio of the mixed fluxes are the welding parameters that significantly affect the quality characteristic; the angle of electrode tip is the most important one as indicated by Table 5.

3.5 Validation of Optimal Welding Conditions

The Taguchi method yielded the welding conditions that optimized the DWR of Inconel 718 alloy welds. The following welding parameters were employed: arc length of 2.0 mm, travel speed of 160 mm/min, flow rate of argon gas 14 L/min, welding current of 180 A, angle of electrode tip of 75°, and the weight ratio of mixed flux, 50% SiO_2 + 50% MoO_3. Figure 7 shows the transverse cross sections of the TIG welds precoated with various compositions and without flux. The penetration capability of TIG welds precoated with flux was obviously higher than that of the welds without flux. In this study, the TIG welds precoated with mixed-component flux 50% SiO_2 + 50% MoO_3 yielded a full penetration under optimal welding conditions. In order to explain and clarify the variation in arc profile, a CCD camera system was used to observe the welding arc as shown in Fig. 8. Due to the constriction of the arc, a smaller anode spot was also observed. Therefore, the effects of plasma column constriction, as well as the consequent increase in current density of the heat source and electromagnetic force of the weld pool, have produced a relatively narrow and deep of weld bead geometry in the TIG welding process.

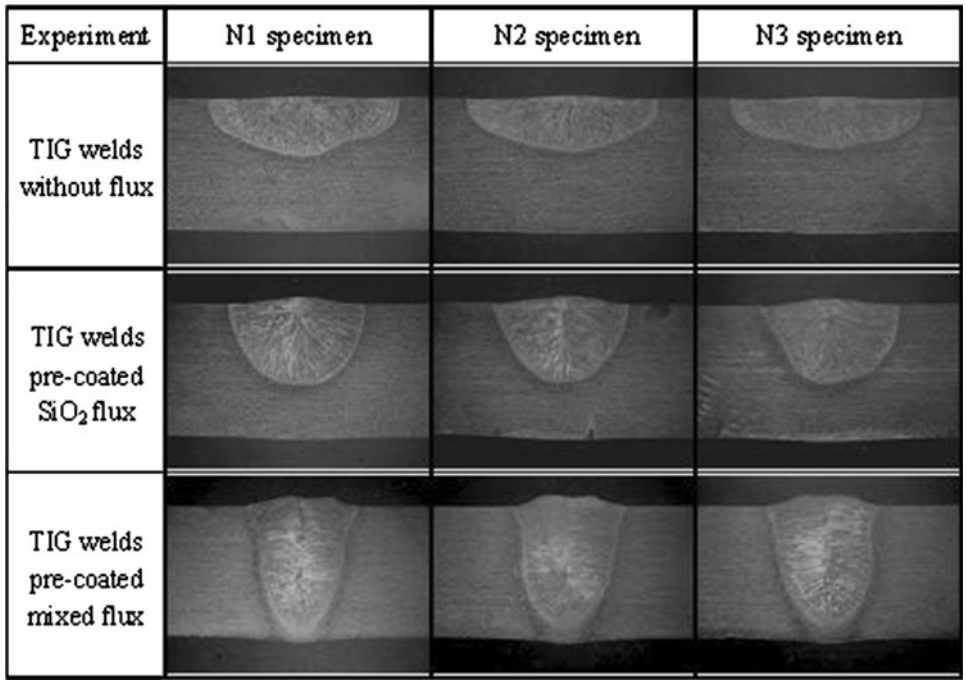

Fig. 7 Effect of activating flux on weld morphology

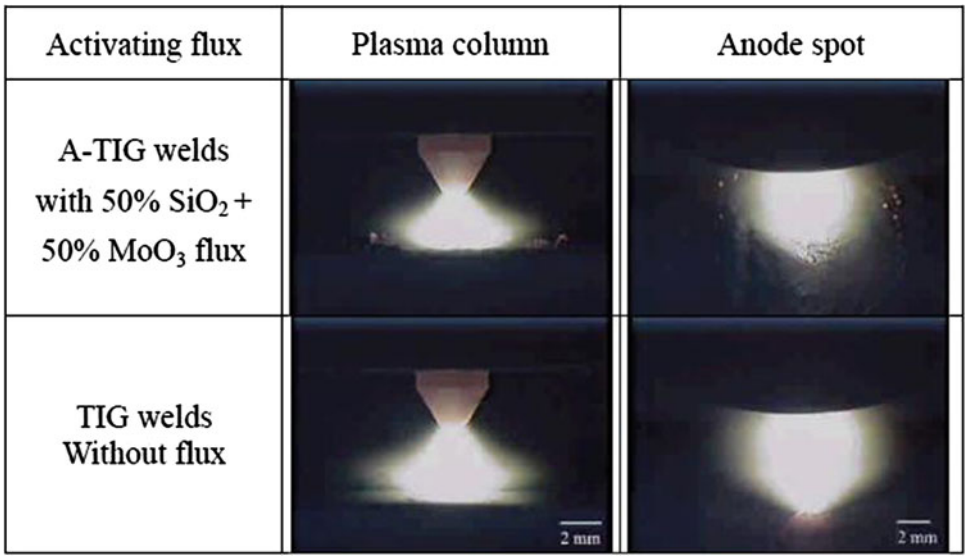

Fig. 8 Images of plasma column and anode spot

4. Conclusions

(1) The voltage of welding arc increases when the Inconel 718 alloy TIG welds produced using activating flux is performed. The fluxes 100% SiO_2, 50% SiO_2 + 50% MoO_3, and 50% SiO_2 + 50% MnS_2 have the significant effects on the voltage of TIG welding arc. The hot cracking susceptibility of Inconel 718 alloy welds is reduced when activating fluxes such as 100% SiO_2 flux, and 50% SiO_2 + 50% MoO_3 fluxes are applied to the TIG welding process.

(2) TIG welds precoated with single-component fluxes such as SiO_2, NiO, and mixed-component fluxes such as 50% SiO_2 +50% MoO_3, 50% SiO_2 + 50% NiO produce a significant increase in the DWR ratio of Inconel 718 alloy welds.

(3) In order to obtain optimal weld bead geometry, considering all the welding parameters, only three parameters play a significant role in this study. The angle of electrode tip is the significant parameter in affecting the DWR of Inconel 718 alloy welds.

(4) TIG welds precoated with 50% SiO_2 + 50% MoO_3 flux under optimal welding conditions not only produce full penetration in 6.35-mm-thickness of Inconel 718 alloy plate, but also decrease the hot cracking susceptibility of Inconel 718 alloy welds.

Acknowledgments

The authors gratefully acknowledge the financial support for this research provided by the National Science Council, Taiwan, Republic of China, under the Grant No. NSC 98-2221-E-539-001.

References

1. C.A. Huang, T.H. Wang, C.H. Lee, and W.C. Han, A Study of the Heat-Affected Zone (HAZ) of an Inconel 718 Sheet Welded with Electron-Beam Welding (EBW), *Mater. Sci. Eng. A*, 2005, **398**, p 275–281
2. R.G. Madhusudhana, M.C.V. Srinivasa, R.K. Srinivasa, and R.K. Prasad, Improvement of Mechanical Properties of Inconel 718 Electron Beam Welds—Influence of Welding Techniques and Postweld Heat Treatment, *Int. J. Adv. Manuf. Technol.*, 2009, **43**, p 671–680
3. S. Gobbi, L. Zhang, J. Norris, K.H. Richter, and J.H. Loreau, High Power CO_2 and Nd-YAG Laser Welding of Wrought Inconel 718, *J. Mater. Process. Technol.*, 1996, **56**, p 333–345
4. R.G.D. Janaki, R.A. Vanugopal, R.K. Prasad, G.M. Reddy, and S.J.K. Sarin, Microstructure and Tensile Properties of Inconel 718 Pulsed Nd-YAG Laser Welds, *J. Mater. Process. Technol.*, 2005, **167**, p 73–82
5. H.B. Cary, *Modern Welding Technology*, 3rd ed., Prentice Hall, Upper Saddle River, NJ, 1994
6. S.C. Juang and Y.S. Tarng, Process Parameter Selection for Optimizing the Weld Pool Geometry in the Tungsten Inert Gas Welding of Stainless Steel, *J. Mater. Process. Technol.*, 2002, **122**, p 33–37
7. D.S. Nagesh and G.L. Datta, Prediction of Weld Bead Geometry and Penetration in Shielded Metal-Arc Welding Using Artificial Neural Networks, *J. Mater. Process. Technol.*, 2002, **123**, p 303–312
8. W. Lucas and D. Howse, Activating Flux-Increasing of Performance and Productivity of the TIG and Plasma Processes, *Weld. Met. Fabr.*, 1996, **64**(1), p 11–17
9. H.Y. Huang, S.W. Shyu, K.H. Tseng, and C.P. Chou, Study of the Process Parameters on Austenitic Stainless Steel by TIG-Flux Welding, *J. Mater. Sci. Technol.*, 2006, **22**(3), p 367–374
10. C.L. Yang, S.B. Lin, F.Y. Liu, L. Wu, and Q.T. Zhang, Research on the Mechanism of Penetration Increase by Flux in A-TIG Welding, *J. Mater. Sci. Technol.*, 2003, **19**(1), p 225–227
11. T.S. Chern, K.H. Tseng, and H.L. Tsai, Study of the Characteristics of Duplex Stainless Steel Activated Tungsten Inert Gas Welds, *Mater. Des.*, 2011, **32**, p 255–263
12. D.L. Olson, T.A. Siewert, S. Liu, and G.R. Edwards (eds.), *Metals Handbook*, vol. 6, (ASM International, Materials Park, Ohio, 1993)
13. A. Koren, M. Roman, I. Weisshaus, and A. Kaufman, Improving the Weldability of Ni-Base Superalloy 713C, *Weld. J.*, 1982, **61**, p 348 s–351 s
14. J. Gordine, Some Problems in Welding Inconel 718, *Weld. J.*, 1971, **50**, p 480 s–484 s
15. S. Leconte, P. Paillard, P. Chapelle, G. Henrion, and J. Saindrenan, Effect of Oxide Fluxes on Activation Mechanisms of Tungsten Inert Gas Process, *Sci. Technol. Weld. Joining*, 2006, **11**(4), p 389–397
16. S. Leconte, P. Paillard, and J. Saindrenan, Effect of Fluxes Containing Oxides on Tungsten Inert Gas Welding Process, *Sci. Technol. Weld. Joining*, 2006, **11**(1), p 43–47
17. Y.L. Xu, Z.B. Dong, Y.H. Wei, and C.L. Yang, Marangoni Convection and Weld Shape Variation in A-TIG Welding Process, *Theoret. Appl. Fract. Mech.*, 2007, **48**, p 178–186
18. C. Limmaneevichitr and S. Kou, Visualization of Marangoni Convection in Simulated Weld Pools Containing a Surface-Active Agent, *Weld. J.*, 2000, **79**, p 324 s–330 s
19. H.L. Lin and C.P. Chou, Optimisation of the GTA Welding Process Using the Taguchi Method and a Neural Network, *Sci. Technol. Weld. Joining*, 2006, **11**(1), p 120–126
20. G. Taguchi, *Taguchi Methods—Design of Experiments*, American Supplier Institute Inc., Michigan, 1993